V European Conference on Computational Fluid Dynamics
ECCOMAS CFD 2010
J. C. F. Pereira and A. Sequeira (Eds)
Lisbon, Portugal,14-17 June 2010

TURBULENT TRANSPORT MODELING FOR PANS AND OTHER BRIDGING CLOSURE APPROACHES

Aditya Murthi*, Dasia A. Reyes*, Sharath S. Girimaji* and Branislav Basara†

*Aerospace Engineering Department
Texas A&M University, College Station, TX, USA
e-mail: girimaji@aero.tamu.edu

†AVL CFD Division
Graz, Austria
e-mail: branislav.basara@avl.com

Key words: Hybrid turbulence modeling, Partially Averaged Navier-Stokes method, Turbulent transport modeling, Scale invariance

Abstract. *Partially Averaged Navier-Stokes (PANS) is a recently developed method for computing turbulent flows. It is purported for smooth bridging between RANS and DNS. Unlike current practice in Large-eddy simulations (LES), PANS entails solving evolution equations for unresolved kinetic energy (K_u) and unresolved dissipation (ϵ_u). One of the most important unclosed terms in PANS is the turbulent transport of K_u and ϵ_u. In this paper, we seek to develop suitable turbulent transport closure models by detailed comparison with numerical and experimental data on benchmark flows. For this purpose, PANS calculations have been performed for a three-dimensional lid-driven cavity flow at Reynolds Number (Re)=10,000 and a three-dimensional circular cylinder at a Reynolds number of (Re)=140,000. The model assessment is based on performance in the following categories:- on (i) mean flow profiles; (ii) resolved flow structure; and (iii) the unresolved-to-resolved kinetic energy (f_k) recovery. We further seek to reaffirm the suitability of PANS as an effective bridging model between RANS and DNS.*

1 INTRODUCTION

One current trend in simulating turbulent flows is the increasing use of seamless bridging methods and zonal hybrid approaches for a variety of practical applications. In the hybrid approach, the modeling challenge is to identify an appropriate criterion for transferring computation from one model to the other while retaining the physical fidelity intact. Due to its very nature, seamless bridging methods do not encounter these difficulties. The closure modeling challenges in the bridging approaches are more similar to that of RANS (Reynolds-averaged Navier-Stokes method). In this paper we will address the turbulent transport modeling of the unresolved kinetic energy and dissipation by unresolved fluctuating scales of motion. Although the model development is in the context of the Partially-averaged Navier-Stokes (PANS: Girimaji, 2006; Girimaji, et al, 2006)[1,2], the methodology and even closure expression should be suitable for all bridging strategies.
Partially-averaged Navier-Stokes (PANS) method is a recently proposed turbulence closure approach, purported for smooth bridging between RANS (Reynolds-averaged Navier-Stokes equations) and DNS (Direct Numerical Simulation).[1] PANS involves solving evolution equations for unresolved kinetic energy (K_u) and unresolved dissipation (ϵ_u). Two of the most important terms that require closure are the turbulent transport of K_u and ϵ_u. The primary purpose of this study is to develop suitable turbulent transport closure models by detailed comparison with experimental and numerical data of Jordan et al[3]. In this regard, PANS calculations have been performed for a *three-dimensional lid-driven cavity* flow at a Reynolds number ($Re = 10,000$) and a *three dimensional circular cylinder* at a Reynolds number ($Re = 140,000$).

Consideration of flow inside a lid-driven cavity for the purpose of turbulent transport development is motivated by three major factors. First, the problem formulation is straight-forward: the geometry is regular and the boundary conditions are well-posed. Second, the lid-driven cavity flow offers the opportunity to study "stationary captive" primary vortices as well as a number of complex secondary phenomena such as the corner vortices and the Taylor-Goertler vortices.[4] As will be shown, turbulent transport models play a crucial role in the resolution of these vortices. Third, the flow is a typical representation of several engineering situations, such as flow over cutouts, slots on walls of heat exchangers, the mixing container of chemical plants etc. Recently, cavity flows have received much attention in acoustics and flame-holding applications.

The flow over a bluff body, such as a 3D cylinder, is also an excellent test bed to develop the transport models. First, there are significant complexities to the flow for which substantial experimental data is available to be used for validation. At this Reynolds number, the flow is considered to be in the sub-critical range. Separation of the flow is laminar and transition to turbulence occurs in the free shear layer in the wake. Second, for the cylinder flow, it is straightforward to determine the ratio of unresolved-to-resolved kinetic energy, or f_k, recovery. The purpose of examining f_k recovery is to determine the consistency of the simulation with user-defined inputs. The details of f_k recovery are

discussed in a subsequent section.

1.1 Experimental and numerical data

On the experimental front, the lid-driven cavity flow has been investigated by a number of researchers: Koseff et. al,[5] Pan et. al[6] and Mills.[7] In a series of insightful papers, Koseff and Street,[5,8,9] present the results from their elaborate measurements to establish the essential features of fully-developed three-dimensional flows in a driven cavity. Flows at several span-to-width ratios (spanwise aspect ratio) were studied. The main observation that emerged from their experiments was that the flows exhibit inherent three-dimensional features with significant transverse motions, the Taylor-Goertler-like (TGL) vortices and end-wall vortices. The visualization studies of Aidun et. al[10] on transition in a cavity of square cross-section but with a spanwise extent three times its height, concluded that this flow becomes unsteady at a Reynolds number of approximately 825 and that the size and number of pairs of TGL vortices depend strongly on the Reynolds number and the Spanwise-Aspect Ratio (SAR).

Numerical investigations carried out by Jordan et. al,[3] include a Direct Numerical Simulation (DNS) at $Re = 5000$ and a Large Eddy Simulation (LES) at $Re = 10,000$, for a SAR of $3:1:1$. At $Re = 5000$, the flow was laminar, in which the three-dimensionality and unsteadiness of the flow resulted in severe distortion of the basic flow structure. Rapid changes in the size of the TGL vortices were noticed and they were shown to meander along the cavity bottom. At higher Reynolds numbers, the vortices themselves became distorted due to the onset of turbulence. Other published results from three-dimensional simulations includes those of Kim et. al,[11] Frietas et. al,[12] and Prasad et. al[13] where the Reynolds number was restricted to low to moderate values ($Re \leq 3200$). In these works, the simulations showed the appearance of quasi-steady and unsteady spanwise TGL vortices along the cavity bottom, which had been observed experimentally.

The flow over a circular cylinder has been well investigated both experimentally and numerically. A high reynolds number experiment was performed by Roshko.[14] Cantwell & Coles[15] performed an experiment for this flow at $Re = 140,000$. At this Reynolds number the flow is considered to be in the sub-critical range. The flow is still laminar when it separates and transition to turbulence occurs in the free shear layer in the wake. This behavior adds significant complexities to the flow. A Reynolds number of 2×10^5-3.5×10^6 is in the critical range. A Reynolds number that is larger than this range is considered to be super-critical. At super-critical Reynolds numbers, the flow turns turbulent prior to separation. The flow stays attached for a longer distance as the turbulent boundary layer is more energetic. Numerical investigations for $Re = 140,000$ include a Detached Eddy Simulation performed by Travin et. al[16] and a Large Eddy Simulation conducted by Breuer.[17] A more detailed literature review can be found in Lakshmipathy[18] covering a range of Reynolds numbers for the cylinder flow problem.

The main objectives of this paper are to develop turbulent transport models for unresolved kinetic energy and dissipation and to perform extensive simulations of three-

dimensional cavity flow and circular cylinder flow for the purpose of transport model validation. The PANS calculations will be compared against LES and experiments whenever possible. We address the following issues:

(i) The effect of turbulent transport models on mean flow profiles.

(ii) The effect of turbulent transport models on resolved flow structure for the lid cavity. As mentioned earlier, it is the presence of primary 'captive vortices', secondary corner and TGL vortices that make the cavity flow an ideal test bed for testing turbulent transport models.

(iii) The effect of turbulent transport model on f_k recovery.

The numerical simulations using PANS is performed for $Re = 10,000$, for a spanwise aspect ratio ($SAR = 2L/W$) of $3:1:1$ for the cavity flow. Simulations have also been performed for other spanwise-aspect ratios such as $0.5:1:1$ and $1:1:1$, but the the results are presented only for the $3:1:1$ case in this paper. The numerical simulation for the cylinder was performed at a Reynolds number of a 140,000.

2 PANS TURBULENCE MODEL

The PANS method used in the current study, has been developed for resolving a portion of the large, unsteady scales of motion ("partial averaging") by making use of the averaging invariance property of the governing equations.[19] In PANS, as in LES, the total field is decomposed into resolved and unresolved parts. PANS, however, is distinctly different from LES in three main aspects: (i) the decomposition is based on the fractions (f_k, f_ϵ) of kinetic energy and dissipation (K_u, ϵ_u) to be modeled and not on the cut-off wavenumber, (ii) PANS filtering (or averaging) is implied rather than explicit and no filtering is performed, and (iii) the SFS (sub-filter scale) stress ($\tau(V_i, V_j)$) is independent of the grid size (Δ): i.e. the level of physical resolution achievable depends wholly, upon the prescription of f_k and f_ϵ and hence is independent of the numerical resolution.
The PANS method is described in detail in Girimaji[1] and the salient features are given below. Starting from the instantaneous incompressible flow equations,

$$\frac{\partial V_i}{\partial t} + V_j \frac{\partial V_i}{\partial x_j} = -\frac{\partial p}{\partial x_i} + \nu \frac{\partial^2 V_i}{\partial x_j \partial x_j} \tag{1}$$

$$\frac{\partial V_i}{\partial x_i} = 0;$$

$\langle\rangle$ a general/arbitrary filtering operator is defined, that is constant preserving and commutes with spatial and temporal differentiation.[1] The instantaneous field can then be decomposed into a filtered field and a residual field:

$$V_i = U_i + u_i \tag{2}$$

where $U_i = \langle V_i \rangle$, corresponds to the filtered field and u_i corresponds to the field that needs to be modeled. On applying such a filtering operator to the instantaneous equations and invoking continuity we get

$$\begin{aligned} \frac{\partial \langle V_i \rangle}{\partial t} + \langle V_j \frac{\partial V_i}{\partial x_j} \rangle &= \frac{\partial \langle V_i \rangle}{\partial t} + \langle V_j \rangle \frac{\partial V_i}{\partial x_j} \\ &\quad + \frac{\partial \tau(V_i, V_j)}{\partial x_j} \end{aligned} \tag{3}$$

In the above equation $\tau(V_i, V_j) = (\langle V_i V_j \rangle - \langle V_i \rangle \langle V_j \rangle)$, is the generalized central moment as defined by Germano.[19] The PANS equation for U_i is then

$$\begin{aligned} \frac{\partial U_i}{\partial t} + U_j \frac{\partial U_i}{\partial x_j} + \frac{\partial \tau(V_i, V_j)}{\partial x_j} &= -\frac{\partial \langle p \rangle}{\partial x_i} + \nu \frac{\partial^2 \langle V_i \rangle}{\partial x_j \partial x_j} \\ &= -\frac{\partial \langle p_u \rangle}{\partial x_i} + \nu \frac{\partial^2 U_i}{\partial x_j \partial x_j} \end{aligned} \tag{4}$$

The pressure field is obtained from

$$\nabla^2 \langle p \rangle = -\frac{\partial U_i}{\partial x_j} \frac{\partial U_j}{\partial x_i} \tag{5}$$

Equation (4) is **unclosed** due to the presence of the sub-filter scale (SFS) stress term $\tau(V_i, V_j)$. The evolution equation for the SFS stress is similar in form to its RANS counterpart:

$$\frac{\partial \tau(V_i, V_j)}{\partial t} + U_k \frac{\partial \tau(V_i, V_j)}{\partial x_k} = P_{ij} + \phi_{ij} - D_{ij} + \mathrm{T_{ij}} \tag{6}$$

where

$$\begin{aligned} P_{ij} &= -\tau(V_i, V_j) \frac{\partial U_j}{\partial x_k} - \tau(V_j, V_k) \frac{\partial U_i}{\partial x_k}; \\ \phi_{ij} &= 2\tau(p', S_{ij}); \quad S_{ij} = \frac{1}{2}\Big(\frac{\partial \langle U_i \rangle}{\partial x_j} + \frac{\partial \langle U_j \rangle}{\partial x_i} \Big) \\ D_{ij} &= 2\nu\tau(\frac{\partial U_i}{\partial x_k}, \frac{\partial U_j}{\partial x_k}); \\ \mathrm{T_{ij}} &= -\frac{\partial}{\partial x_k}\Big(\tau(V_i, V_j, V_k) + \tau(p, V_j)\delta_{ik} \\ &\quad -\nu \frac{\partial \tau(V_i, V_j)}{\partial x_k} \Big) \end{aligned} \tag{7}$$

are the terms for production, pressure-strain correlation, dissipation and transport of SFS stresses respectively. In the above, p' is the pressure field corresponding to unresolved fluctuations:

$$\nabla^2 p' = -2\frac{\partial U_i}{\partial x_j} \frac{\partial u_j}{\partial x_i} - \frac{\partial u_i}{\partial x_j} \frac{\partial u_j}{\partial x_i} \tag{8}$$

From equation (6), we observe that its form is invariant to the type of filter and consequently, the SFS stress model form must be **invariant** to the type of averaging, provided the generalized central moments are used.[19] Based on these arguments, PANS is capable of inheriting its model form from either RANS or LES. However, since most current subgrid LES closures are zero-equation models, they are too elementary to be used as a basis for PANS.

In PANS, the extent of filtering is quantified by specifying the ratios of unresolved kinetic energy and dissipation[1]

$$f_k = \frac{K_u}{K} \quad f_\epsilon = \frac{\epsilon_u}{\epsilon}. \tag{9}$$

In the above equation K and ϵ are the total kinetic energy and dissipation.

2.1 RANS-type sub-filter stress closure

A Boussinesq-type approximation or mixing-length arguments can be used for partial fields as well.[1] The SFS stress term $\tau(V_i, V_j)$ can be chosen in equation (6) according to

$$\tau(V_i, V_j) = -\nu_u\Big(\frac{\partial U_i}{\partial x_j} + \frac{\partial U_j}{\partial x_i}\Big) + \frac{2}{3}K_u\delta_{ij} \tag{10}$$

where $\nu_u = C_\mu \frac{K_u^2}{\epsilon_u}$. From the above equation, it is observed that in order to completely close the SFS stress term, suitable models for K_u and ϵ_u have to be prescribed. In Girimaji[1] the starting point for this development is the RANS two-equation $K-\epsilon$ model:

$$\begin{aligned} \frac{\partial K}{\partial t} + \overline{U_j}\frac{\partial K}{\partial x_j} &= P - \epsilon + \frac{\partial}{\partial x_j}\Big(\frac{\nu_t}{\sigma_k}\frac{\partial K}{\partial x_j}\Big) \\ \frac{\partial \epsilon}{\partial t} + \overline{U_j}\frac{\partial \epsilon}{\partial x_j} &= C_{\epsilon 1}\frac{P\epsilon}{K} - C_{\epsilon 2}\frac{\epsilon^2}{K} \\ &\quad + \frac{\partial}{\partial x_j}\Big(\frac{\nu_t}{\sigma_\epsilon}\frac{\partial \epsilon}{\partial x_j}\Big) \end{aligned} \tag{11}$$

where $\overline{U}$ is the mean velocity, P is the production of kinetic energy, ϵ is the dissipation-rate, ν_t is the total turbulent viscosity ($\nu_t = C_\mu \frac{K^2}{\epsilon}$) and $C_{\epsilon 1}$, $C_{\epsilon 2}$ are model coefficients.

The model equations for K_u and ϵ_u are derived by considering the following requirements:

(i) The ratios of unresolved to total kinetic energy and dissipation must be equal to f_k and f_ϵ respectively.

(ii) PANS must reduce to RANS as f_k and f_ϵ tend to unity.

(iii) PANS must reduce to DNS as f_k and f_ϵ tend to zero.

In summary, f_k and f_ϵ serve as resolution control parameters for obtaining the desired level of resolution. Based on the above requirements, the model equation for K_u is derived by Girimaji[1]

$$\begin{aligned}\frac{\partial K_u}{\partial t}+U_j\frac{\partial K_u}{\partial x_j} &= P_u-\epsilon_u+\frac{\partial}{\partial x_j}\Big(\frac{\nu_t}{\sigma_k}\frac{\partial K_u}{\partial x_j}\Big) \\ &\quad +(U_j-\overline{U_j})\frac{\partial K_u}{\partial x_j}\end{aligned} \tag{12}$$

where $P_u=\tau(V_i,V_j)\frac{\partial U_i}{\partial x_j}$ corresponds to unresolved production, ϵ_u the unresolved dissipation and T_{k_u} the transport of unresolved kinetic energy. The above equation is identical to the equation for kinetic energy K, but for the additional transport term involving convection of unresolved energy by resolved fluctuations $(U_j-\overline{U_j})$.
The model equation for ϵ_u is developed in a similar fashion by requiring that

$$\frac{d\epsilon_u}{dt}=f_\epsilon\frac{d\epsilon}{dt} \tag{13}$$

which leads to

$$\begin{aligned}\frac{\partial \epsilon_u}{\partial t}+U_j\frac{\partial \epsilon_u}{\partial x_j} &= C_{\epsilon1}\frac{P_u\epsilon_u}{K_u}-\Big(C_{\epsilon1}+\frac{f_k}{f_\epsilon}(C_{\epsilon2}-C_{\epsilon1})\Big)\frac{\epsilon_u^2}{K_u} \\ &\quad +\frac{\partial}{\partial x_j}\Big(\frac{\nu_t}{\sigma_\epsilon}\frac{\partial \epsilon_u}{\partial x_j}\Big)+(U_j-\overline{U_j})\frac{\partial \epsilon_u}{\partial x_j}\end{aligned} \tag{14}$$

Finally, the two-equation PANS model can be summarized as follows:

$$\begin{aligned}\frac{\partial K_u}{\partial t}+U_j\frac{\partial K_u}{\partial x_j} &= P_u-\epsilon_u+T_{k_u} \\ \frac{\partial \epsilon_u}{\partial t}+U_j\frac{\partial \epsilon_u}{\partial x_j} &= C_{\epsilon1}\frac{P_u\epsilon_u}{K_u}-C^*_{\epsilon2}\frac{\epsilon_u^2}{K_u}+T_{\epsilon_u}\end{aligned} \tag{15}$$

where

$$C^*_{\epsilon2}=\Big(C_{\epsilon1}+\frac{f_k}{f_\epsilon}(C_{\epsilon2}-C_{\epsilon1})\Big) \tag{16}$$

and $C_{\epsilon1}$ and $C_{\epsilon2}$ are the standard $K-\epsilon$ model constants. The two terms for turbulent transport of unresolved quantities T_{K_u} and T_{ϵ_u} are expressed as

$$\begin{aligned}T_{k_u} &= \frac{\partial}{\partial x_j}\Big(\frac{\nu_t}{\sigma_k}\frac{\partial K_u}{\partial x_j}\Big)+(U_j-\overline{U_j})\frac{\partial K_u}{\partial x_j} \\ &= \frac{\partial}{\partial x_j}\Big(\frac{\nu_t}{\sigma_k}\frac{\partial K_u}{\partial x_j}\Big)+D_{k_u} \\ T_{\epsilon_u} &= \frac{\partial}{\partial x_j}\Big(\frac{\nu_t}{\sigma_\epsilon}\frac{\partial \epsilon_u}{\partial x_j}\Big)+(U_j-\overline{U_j})\frac{\partial \epsilon_u}{\partial x_j} \\ &= \frac{\partial}{\partial x_j}\Big(\frac{\nu_t}{\sigma_\epsilon}\frac{\partial \epsilon_u}{\partial x_j}\Big)+D_{\epsilon_u}\end{aligned} \tag{17}$$

where D_{k_u} and D_{ϵ_u} represent the transport of kinetic energy and dissipation by resolved-scale fluctuations. From the above equations it is observed that the only terms that require further closure are these transport terms.

3 TURBULENT TRANSPORT MODELS

The physics of T_{k_u} can be understood as follows. The first term is in equation (17) is the RANS turbulent transport which represents the transport of K_u by all fluctuations. In PANS, the transport due to the resolved fluctuations $(\overline{U_j} - U_j)$ is already included in the advection term. Therefore, in PANS only the transport due to unresolved fluctuations should appear in the turbulent transport term. Hence, the PANS turbulent transport (T_{k_u}) must be surmised by subtracting the transport due to resolved scales (D_{k_u}) from the total transport due to all scales $\left(\frac{\partial}{\partial x_j}\left(\frac{\nu_t}{\sigma_k}\frac{\partial K_u}{\partial x_j}\right)\right)$. A similar explanation is valid for the PANS turbulent transport of ϵ_u as well.

The equations for T_{k_u} and T_{ϵ_u} i.e. (17), can be written fully in terms of PANS variables as

$$\begin{aligned} T_{k_u} &= \frac{\partial}{\partial x_j}\left(\frac{\nu_t}{\sigma_k}\frac{\partial K_u}{\partial x_j}\right) - (\overline{U_j} - U_j)\frac{\partial K_u}{\partial x_j} \\ &= \frac{\partial}{\partial x_j}\left(\frac{\nu_u f_\epsilon}{\sigma_k f_k^2}\frac{\partial K_u}{\partial x_j}\right) - D_{k_u} \end{aligned} \tag{18}$$

$$\begin{aligned} T_{\epsilon_u} &= \frac{\partial}{\partial x_j}\left(\frac{\nu_t}{\sigma_\epsilon}\frac{\partial \epsilon_u}{\partial x_j}\right) - (\overline{U_j} - U_j)\frac{\partial \epsilon_u}{\partial x_j} \\ &= \frac{\partial}{\partial x_j}\left(\frac{\nu_u f_\epsilon}{\sigma_\epsilon f_k^2}\frac{\partial \epsilon_u}{\partial x_j}\right) - D_{\epsilon_u} \end{aligned}$$

as the RANS and PANS eddy viscosities are related according to

$$\nu_u = C_\mu \frac{K_u^2}{\epsilon_u} = C_\mu \frac{f_k^2}{f_\epsilon}\frac{K^2}{\epsilon} = \frac{f_k^2}{f_\epsilon}\nu_t \tag{19}$$

It is clear that modeling of T_{k_u} and T_{ϵ_u} reduces to modeling D_{k_u} and D_{ϵ_u}. We propose that this transport should be amenable to gradient transport modeling. We now investigate two possible gradient transport models: the Zero-transport model (ZTM) and the Maximum transport model (MTM).

Zero-transport Model: In this model, it is assumed that resolved fluctuations $(\overline{U_j} - U_j)$ do not contribute to the net transport of the quantity in question.

$$D_q \equiv (\overline{U_j} - U_j)\frac{\partial q}{\partial x_j} \approx 0 \tag{20}$$

where q is any quantity of interest; K_u or ϵ_u. If ZTM is invoked for K_u or ϵ_u we will have

$$T_{k_u} = \frac{\partial}{\partial x_j}\Big(\frac{\nu_u f_\epsilon}{\sigma_k f_k^2}\frac{\partial K_u}{\partial x_j}\Big) = \frac{\partial}{\partial x_j}\Big(\frac{\nu_u}{\sigma_{k_u}}\frac{\partial K_u}{\partial x_j}\Big) \tag{21}$$

$$T_{\epsilon_u} = \frac{\partial}{\partial x_j}\Big(\frac{\nu_u f_\epsilon}{\sigma_\epsilon f_k^2}\frac{\partial \epsilon_u}{\partial x_j}\Big) = \frac{\partial}{\partial x_j}\Big(\frac{\nu_u}{\sigma_{\epsilon_u}}\frac{\partial \epsilon_u}{\partial x_j}\Big)$$

with the unresolved Prandtl numbers defined as

$$\begin{aligned} \sigma_{k_u} &\equiv \frac{f_k^2}{f_\epsilon}\sigma_k \\ \sigma_{\epsilon_u} &\equiv \frac{f_k^2}{f_\epsilon}\sigma_\epsilon \end{aligned} \tag{22}$$

Maximum transport model:- In this model it is assumed that the resolved fluctuation do contribute to net transport. The effective viscosity of this transport is taken to be the difference between total eddy viscosity and the unresolved eddy viscosity:

$$\nu_r = \nu_t - \nu_u = C_\mu\frac{K^2}{\epsilon} - C_\mu\frac{K_u^2}{\epsilon_u} \tag{23}$$

If this assumption is invoked we will have

$$(\overline{U_j} - U_j)K_u = \Big(\frac{\nu_r}{\sigma_k}\frac{\partial K_u}{\partial x_j}\Big) = \Big(\frac{(\nu_t - \nu_u)}{\sigma_k}\frac{\partial K_u}{\partial x_j}\Big), \tag{24}$$

$$(\overline{U_j} - U_j)\epsilon_u = \Big(\frac{\nu_r}{\sigma_k}\frac{\partial \epsilon_u}{\partial x_j}\Big) = \Big(\frac{(\nu_t - \nu_u)}{\sigma_k}\frac{\partial \epsilon_u}{\partial x_j}\Big).$$

Then the expressions for transport quantities D_{k_u} and D_{ϵ_u} are

$$\begin{aligned} D_{k_u} &= \frac{\partial}{\partial x_j}(\overline{U_j} - U_j)K_u = \frac{\partial}{\partial x_j}\Big(\frac{\nu_r}{\sigma_k}\frac{\partial K_u}{\partial x_j}\Big) \\ &= \frac{\partial}{\partial x_j}\Big(\frac{(\nu_t - \nu_u)}{\sigma_k}\frac{\partial K_u}{\partial x_j}\Big) \end{aligned} \tag{25}$$

$$\begin{aligned} D_{\epsilon_u} &= \frac{\partial}{\partial x_j}(\overline{U_j} - U_j)\epsilon_u = \frac{\partial}{\partial x_j}\Big(\frac{\nu_r}{\sigma_\epsilon}\frac{\partial \epsilon_u}{\partial x_j}\Big) \\ &= \frac{\partial}{\partial x_j}\Big(\frac{(\nu_t - \nu_u)}{\sigma_\epsilon}\frac{\partial \epsilon_u}{\partial x_j}\Big) \end{aligned}$$

Upon substituting the above results into equation (18) we get

$$\begin{aligned} T_{k_u} &= \frac{\partial}{\partial x_j}\Big(\frac{\nu_t}{\sigma_k}\frac{\partial K_u}{\partial x_j}\Big) - \frac{\partial}{\partial x_j}\Big(\frac{(\nu_t-\nu_u)}{\sigma_k}\frac{\partial K_u}{\partial x_j}\Big) \\ &= \frac{\partial}{\partial x_j}\Big(\frac{\nu_u}{\sigma_k}\frac{\partial K_u}{\partial x_j}\Big) \\ &= \frac{\partial}{\partial x_j}\Big(\frac{\nu_u}{\sigma_{k_u}}\frac{\partial K_u}{\partial x_j}\Big) \end{aligned} \tag{26}$$

and

$$\begin{aligned} T_{\epsilon_u} &= \frac{\partial}{\partial x_j}\Big(\frac{\nu_t}{\sigma_\epsilon}\frac{\partial \epsilon_u}{\partial x_j}\Big) - \frac{\partial}{\partial x_j}\Big(\frac{(\nu_t-\nu_u)}{\sigma_\epsilon}\frac{\partial \epsilon_u}{\partial x_j}\Big) \\ &= \frac{\partial}{\partial x_j}\Big(\frac{\nu_u}{\sigma_\epsilon}\frac{\partial \epsilon_u}{\partial x_j}\Big) \\ &= \frac{\partial}{\partial x_j}\Big(\frac{\nu_u}{\sigma_{\epsilon_u}}\frac{\partial \epsilon_u}{\partial x_j}\Big) \end{aligned} \tag{27}$$

with the modified Prandtl numbers defined as

$$\begin{aligned} \sigma_{k_u} &\equiv \sigma_k \\ \sigma_{\epsilon_u} &\equiv \sigma_\epsilon. \end{aligned} \tag{28}$$

A priori assessment of models:- Preliminary evaluation of the two models can be performed with simple mixing length arguments such as described in Tennekes and Lumley[20]. The net transport of a quantity (q) by a velocity field depends on the length scales of the two fields. If the length-scales of the q and $(\underline{U}-\overline{\underline{U}})$ fields are very different, then the net transport will be small due to lack of correlation between the two fields. Conversely, the most efficient transport occurs when the transported quantity and the transporting velocity field are of similar length scales.

In the current case, three length scales are of interest: $L-$ integral length scale of turbulence; $\eta-$ the Kolmogorov length scale; and l_c- the implied PANS cut-off scale. The range of scales in the various fields are

(i) Length-scale of $(\overline{U_j}-U_j) \sim (L, l_c)$

(ii) Length-scale of $K_u \sim (l_c, \eta)$

(iii) Length-scale of ϵ_u fields $\sim \eta$.

Clearly $L > l_c > \eta$.

Since there is no overlap between the length-scales of $(\underline{U}-\overline{\underline{U}})$ and ϵ_u, we expect the ZTM to be more appropriate: $D_{\epsilon_u} \approx 0$. Since there is some overlap between the velocity

and the K_u scales (in the proximity of l_c), we expect some net transport. Hence ZTM or MTM maybe appropriate for unresolved kinetic energy K_u. Our objective is to assess these models in the 3-D lid-driven cavity flow and flow past a circular cylinder. However, at small Reynolds numbers there may not be a big demarcation between the scales and MTM may be more appropriate.

4 COMPUTATIONAL ISSUES

The **FLUENT** flow solver has been used to perform the PANS calculations for the cavity and cylinder flows. It is important to note that **FLUENT** is originally intended for RANS. However, PANS calculations are made by suitably changing the values of the model coefficient $C_{\epsilon 2}$ and Prandtl numbers σ_k and σ_ϵ.

The cavity geometry considered has a spanwise aspect ratio (SAR) of 3:1:1, for which qualitative as well as quantitative data are available for comparison.[3] The width(W) and the height(H) are taken to be 1.0, in both x and y directions and the span(L) is taken to be 1.5 in the z-direction. One boundary of the span (L) is treated as the plane of symmetry (z=0.0) and the other as a solid end-wall. The symmetry condition was used as it yielded accurate statistics at half the computational expense of a full geometry simulation. The LES data in Jordan et. al[3] that have been used for current model comparisons, has also been generated by utilizing this condition. The lid (top wall) is prescribed a velocity(U) of 1 m/s in the horizontal direction. Simulations are performed for a Reynolds number of 10,000. Sampling for statistics is not enabled until ten cycles (corresponding to 60 seconds of flow time) are completed in order for the flow to become fully-developed. The grid sizes used for the simulations for different f_k values are shown in Table I.

	f_k	Grid Sizes
1	0.2	95x95x95
2	0.4	81x81x81
3	0.5	75x75x75
4	0.7	64x64x64
5	1.0	51x51x51

Table 1: Grid sizes for various f_k calculations

For the cylinder calculation, the length of the width and height are 15d and the span is 2d, where d is the diameter of the cylinder. The grid size is 320 x 240 x 32. The f_k values tested for the cylinder are 0.4 and 0.6. In previous work, grid and temporal refinement studies were performed with PANS for the cylinder flow problem at a Reynolds number of 140,000 with the same dimensions of the domain studied here. The grid refinement study showed that the results did not change for grids finer than 140 x 120 x 32. It is assumed that the grid used in this simulation is sufficient for f_k values of 0.4 and 0.6, since it is significantly finer than the one found to be appropriate for a PANS simulation performed at $f_k = 0.5$. Similarly, a temporal refinement study was performed for this

cylinder problem. It was found that a δt value of 0.0525 was sufficient for both f_k values. Using the previous argument, the δt must be decreased for a f_k value of 0.4. In all the simulations a time step of 0.025 is used.[18] Sampling for mean statistics was enabled after 10,000 iterations which corresponded to a flow time of 100 seconds. In all the computations for the lid cavity and cylinder we use $f_\epsilon = 1$.

5 RESULTS AND DISCUSSION

In this section, the results of simulations conducted using the Zero-transport (ZTM) and the Maximum transport (MTM) models are presented. Comparisons with data for the lid cavity[2] and circular cylinder[14] are made to assess model performances. The plots for statistical quantities along cavity centerlines have been generated by sampling every 6.5 seconds, after statistical steady state is reached. Statistical sampling for the cylinder is taken after steady state behavior has been achieved in the flow and then sampling is taken every second for 100 seconds. Results have been presented for f_k values of 1.0 (RANS), $0.7, 0.4$ and 0.2 for the cavity flow. The cylinder results include f_k values of 1.0, 0.6 and 0.4.

It is important to ensure that the transport model preserves the desired level of resolution. This will be accomplished by comparing the ratio of the PANS turbulent viscosity at each point in the domain to that of the RANS turbulent viscosity at that same point. The pdf of this plot will show how much of the flow is actually consistent with the specified f_k value. The ratio of the turbulent viscosity is the following:

$$\frac{\nu_u}{\nu_t} = \frac{f_k^2}{f_\varepsilon} \tag{29}$$

5.1 Mean flow profiles

The first set of figures show mean velocity comparisons of the two transport models along with LES and experiment data of the cavity flow. In figures 1a and 1b, the mean U and V velocity profiles obtained from RANS, LES and experiment are shown. It is evident that RANS performance is inferior to that of LES and experiments. Figures 2a (Mean U velocity) and 2b (Mean V velocity) present comparisons of PANS-MTM with RANS, LES and experiment for f_k values - $0.2, 0.4$ and 0.7. It is observed that MTM performs better than RANS and shows better convergence towards LES (and experiment), with $f_k = 0.2$ being most accurate in its predictions. The next set of figures 3a and 3b show comparisons of PANS-ZTM with RANS, LES and experiments. ZTM also shows very good agreement with data, and the $f_k = 0.2$ case is nearly as accurate as LES. Upon comparing figures 2 and 3, it is observed that ZTM is closer with LES and experiment than MTM for corresponding values of f_k. This trend is especially evident near the cavity boundaries as seen in the figures.

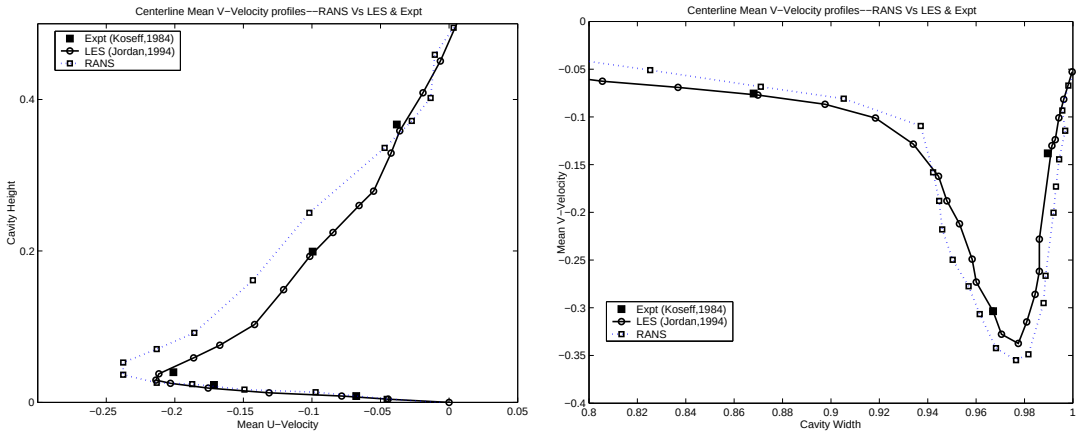

(a) Bottom wall closeup (b) Downstream wall closeup

Figure 1: Mean V-Velocity profiles, RANS vs LES and experiment

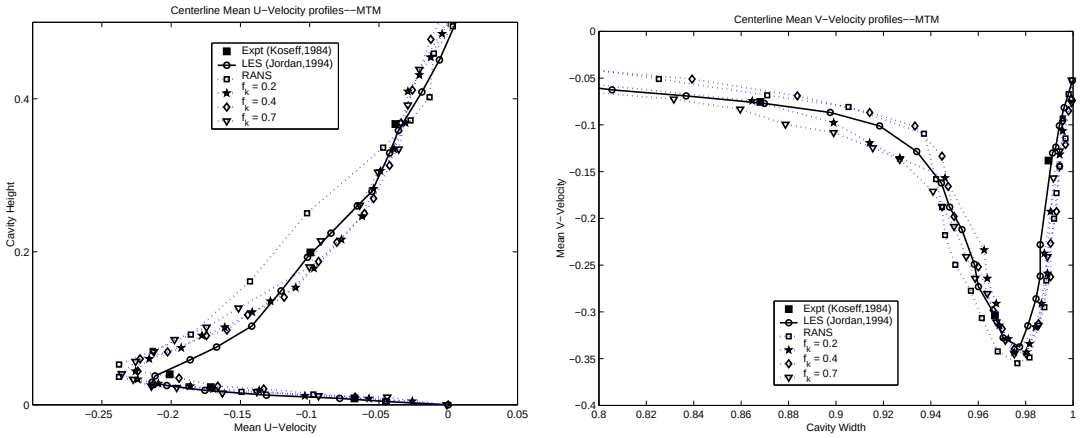

(a) Bottom wall closeup (b) Downstream wall closeup

Figure 2: Mean V-Velocity profiles, MTM

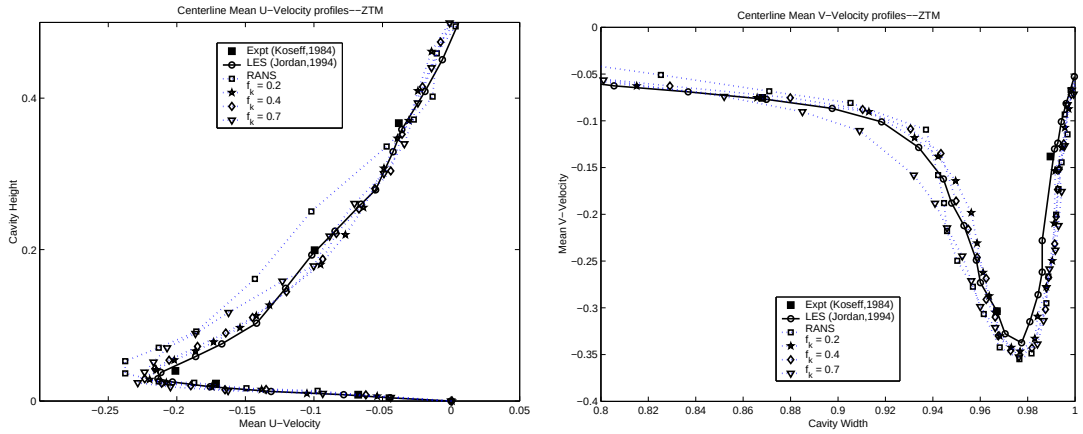

(a) Bottom wall closeup (b) Downstream wall closeup

Figure 3: Mean V-Velocity profiles, ZTM

For the circular cylinder, the ZTM simulations do not accurately capture the mean x-velocity profile of the near wake region at x/D=1.0, as shown in figure 4a. It also appears that the RANS simulation performs slightly better in the region directly aft of the cylinder. The PANS simulations do provide significant improvement over the RANS simulation in capturing this profile in the near wake region at $x/D = 3$ seen in figure 5a and at the wake centerline seen in figure 6a. From these observations, it can be concluded that the PANS simulations performs better in the far wake region than they do in the near wake region. Also, another important observation is that there is not a distinct difference between the ability of the PANS $f_k = 0.4$ and $f_k = 0.6$ simulations to capture the mean statistics. In other words, the physics of circular cylinder flow can be captured with the $f_k = 0.6$ resolution at nearly the same quality of agreement as the $f_k = 0.4$ simulation.

In the MTM simulations for the cylinder flow, there is little difference between RANS simulation of $f_k = 1$ and the PANS simulations of $f_k = 0.4$ and 0.6 for capturing the mean statistics in the near wake region at x/D=1.0 seen in figure 4b. In this near wake region, when utilizing MTM, it can be concluded that the PANS simulations behave like RANS. The poor results shown with MTM are expected because in the near wake region the Reynolds number is higher and ZTM should be more appropriate. Further in the wake, the Reynolds number decreases and the MTM model should provide more accurate results. Improvement in capturing experimental results using MTM is indeed seen in the plots of the near wake region at x/D=3.0 (figure 5b) and at the wake centerline (figure 6b). In figure 8b, the $f_k = 0.4$ and $f_k = 0.6$ show vast improvement over the RANS case. The $f_k = 0.4$ case shows the best recovery. The PANS simulations also show improvement over the RANS case in capturing the mean velocity profile at the wake centerline as can be seen in figure 6c.

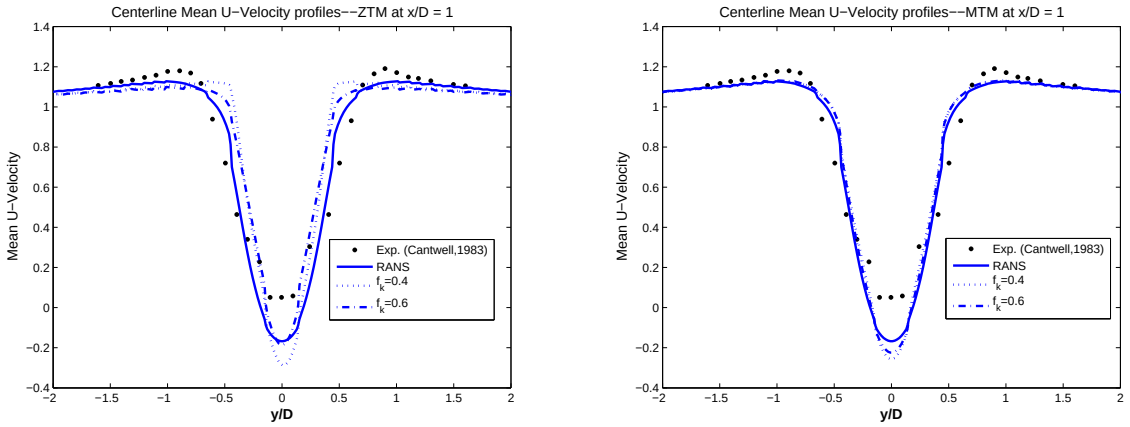

(a) ZTM (b) MTM

Figure 4: Mean U-Velocity profiles at x/D=1

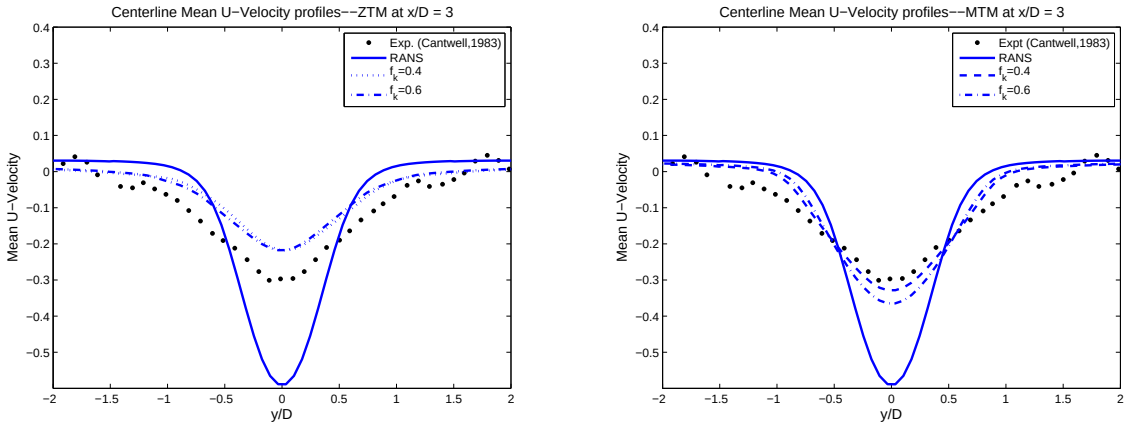

(a) ZTM (b) MTM

Figure 5: Mean U-Velocity profiles at x/D=3

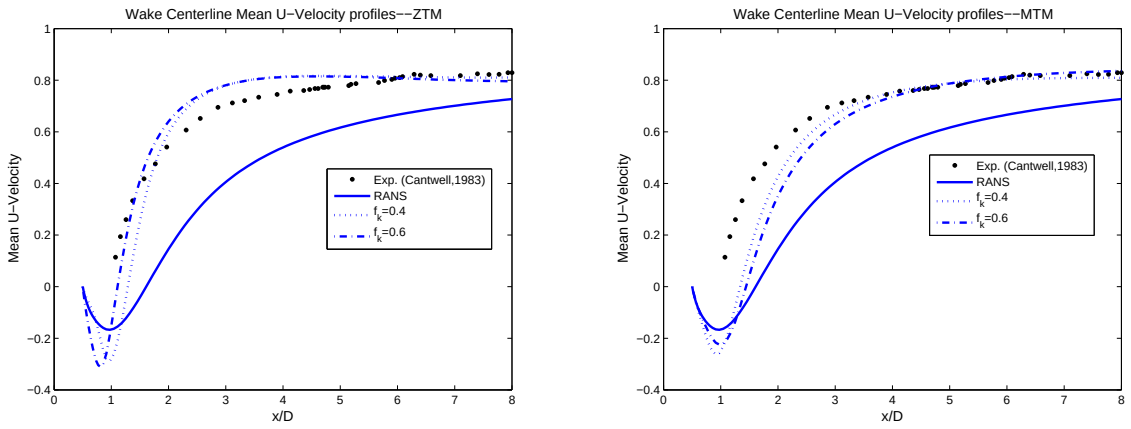

(a) ZTM (b) MTM

Figure 6: Mean U-Velocity profiles in wake

5.2 Resolved flow structure

Figures 7 and 8 display contours of X-vorticity according to MTM and ZTM, for $f_k = 0.7$ and 0.4. Figures 7a and 7b ($f_k = 0.7$) show considerably more scales of flow are resolved by ZTM when compared to MTM, in terms of appearance of Taylor Goertler-like (TGL) vortex pairs. About three pairs of TGL vortices are observed for ZTM while only one pair can be seen for MTM. As the value of f_k is reduced, more and more pairs of vortices are uncovered and the number of flow features resolved by ZTM is considerably more than that for MTM, for a given f_k. Specifically, 5 pairs of TGL vortices are observed for ZTM (Figure 8a) as against 3 pairs for MTM (Figure 8b), for $f_k = 0.4$. Overall, the ZTM results are in better qualitative agreement than MTM calculations.

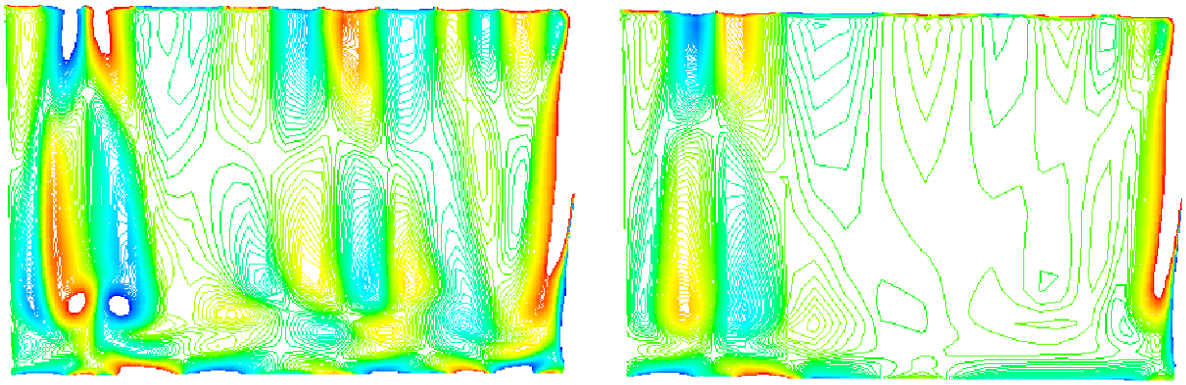

(a) ZTM (b) MTM

Figure 7: X-Vorticity contours along downstream wall, $f_k = 0.7$

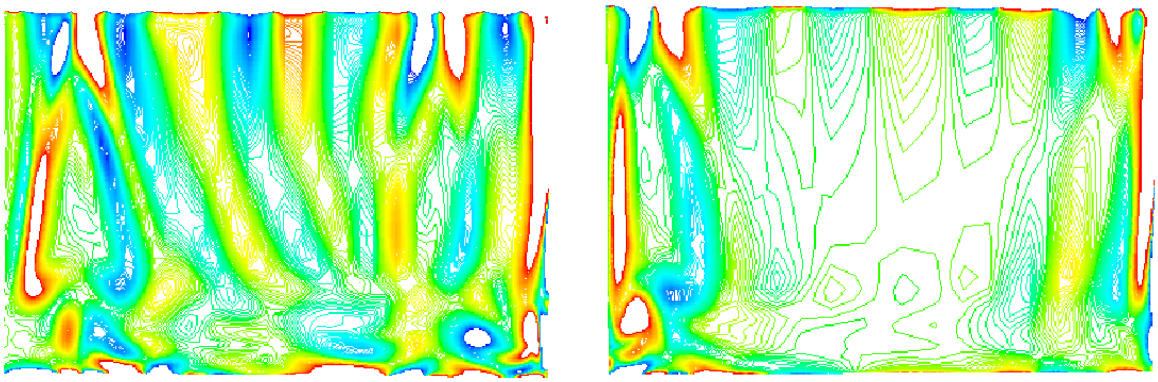

(a) ZTM (b) MTM

Figure 8: X-Vorticity contours along downstream wall, $f_k = 0.4$

5.3 f_k recovery

The purpose of performing this study is to determine if the PANS simulation is self-consistent with the specified f_k value. As shown in Lakshmipathy and Girimaji this represents a key step in validating the closure models used in PANS.[21] For the f_k values of 0.4 and 0.6, the pdf of the viscosity ratio should peak at 0.16 and 0.36, respectively, as the ratio is proportional to f_k^2. The MTM does not show good recovery of the specified viscosity ratio and fails the internal validation test. The conclusion from this study of the ZTM and MTM approaches is summarized as follows. The ZTM model is more accurate

for this problem at this Reynolds number because it preserves internal consistency and provides reasonably accurate results in the near wake region.[22]

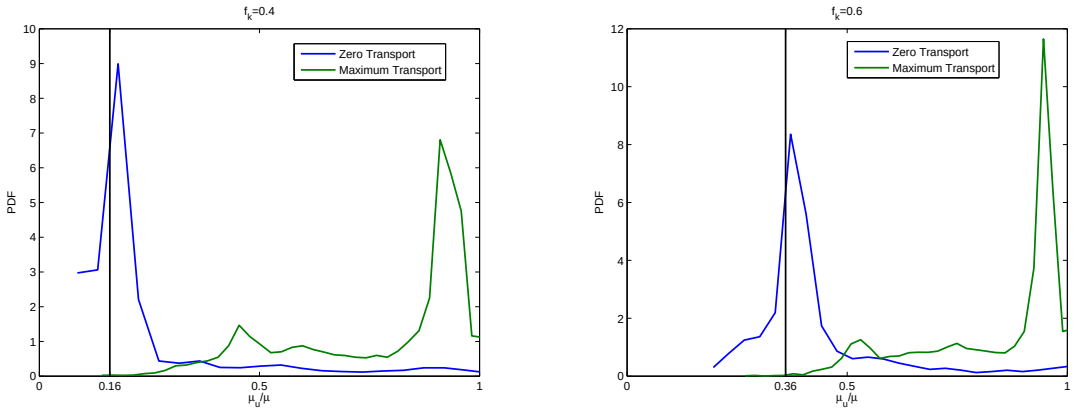

(a) $f_k = 0.4$ (b) $f_k = 0.6$

Figure 9: f_k Recovery

6 CONCLUSIONS AND SUMMARY

In the present study, a detailed numerical investigation of the three-dimensional lid-driven cavity flow and circular cylinder flow are carried out using a new turbulence modeling technique, know as the Partially Averaged Navier-Stokes method or PANS. Flow studies have been conducted at $Re = 10,000$ on a three-dimensional lid-driven cavity for a spanwise aspect ratio (SAR) of 3:1:1, with the top surface imparted with a constant velocity of 1 m/s. The circular cylinder flow studies are performed for a $Re = 140,000$. The investigation primarily focuses on the effect of two turbulent transport models: the Zero-transport model (ZTM) and the Maximum transport model (MTM), on PANS calculations to ascertain which model performs better for K_u and ϵ_u.

The main conclusions that can be drawn by observing the lid cavity results are: (i) as the value of f_k is decreased from 1 (RANS) to 0 (DNS) more scales of flow are resolved in terms of the appearance of flow features, such as the TGL vortices, as evident from the contour plots of X-vorticity, and (ii) in general, the Zero-transport model appears to perform better than the Maximum transport model as inferred from the mean velocity profiles. Specifically, ZTM appears to be better suited for modeling unresolved dissipation ϵ_u, while the both models seem adequate for unresolved kinetic energy K_u.

For the circular cylinder flow, it appears that ZTM is the more appropriate transport model for this Reynolds number. The performance of MTM is better in the far wake than in the near wake. The simulation for the ZTM model is consistent with the specified f_k value as reflected in the f_k recovery plot. In this context, it seems reasonable to conclude that PANS is capable of serving as a **bridging model** between RANS and DNS.

REFERENCES

[1] Girimaji, S. S. 2006 Partially-averaged Navier-Stokes method for turbulence: A Reynolds-averaged Navier-Stokes to direct numerical simulation bridging method, *Journal of Applied Mechanics*, **73**, 413-421.

[2] Girimaji, S., Jeong, E. & Srinivasan, R. 2006 Partially averaged Navier-Stokes method for turbulence: Fixed point analysis and comparison with unsteady partially averaged Navier-Stokes, *Journal of Applied Mechanics*, **73**, 422-429.

[3] Jordan, S. A. & Ragab, S. A. 1994 On the Unsteady and Turbulent Characteristics of Three-Dimensional Shear-Driven Cavity Flow, *Journal of Fluids Engineering*, **116**, 439-449.

[4] Roshko, A. 1955 NACA Tech. Notes, No. 3488.

[5] Koseff, J. R., and Street, R. L., 1984 Visualization Studies of a Shear Three- Dimensional Recirculation Flow, *ASME J. Fluid. Eng.*, **Vol. 106**, No. 1, pp. 21- 29.

[6] Pan, F. & Acrivos, A. 1967 Steady Flows in Rectangular Cavities, *J. Fluid. Mech*, **Vol. 28**, pp. 643-655.

[7] Mills, R. D.1965 Numerical Solutions of the Viscous Equations for a Class of Closed Flows, *J. Roy. Aero. Soc.*, **69**, pp. 714-718.

[8] Koseff, J. R. & Street, R. L. 1984 On End-Wall Effects in a Lid-Driven Cavity Flow, *ASME J. Fluid. Eng.*, **Vol. 106**, No. 1, pp. 385-389.

[9] Koseff, J. R. & Street, R. L. 1984 The Lid-Driven Cavity Flow: A Synthesis of Qualitative and Quantitative Observations, *ASME J. Fluid. Eng.*, **Vol. 106**, No. 1, pp. 390-398.

[10] Aidun, C. K., Triantafillopoulos, N. G. & Benson, J. D. 1991 Global stability of a Lid-Driven Cavity with through flow: Flow visualization studies, *Physics of Fluids A*, **Vol. 3**, pp. 2081-2091.

[11] Kim, J. & Moin, P. 1985 Application of a Fractional-Step Method to Incom- pressible Navier-Stokes Equations, *Journal of Computational Physics*, **Vol. 59**, pp. 308-310.

[12] Frietas, C. J., Street, R. L., Findikakis, A. N. & Koseff, J. R. 1985 Numerical Simulation of Three-Dimensional Flow in a Cavity, *International Journal of Numerical Methods in Fluids*, **Vol. 5**, No. 6, pp. 561-576.

[13] Prasad, A. K. & Koseff, J. R. 1989 Reynolds Number and End-Wall Effects on a Lid-Driven Cavity Flow, *Physics of Fluids*, **Vol. 1**, No. 2, pp. 208-218.

[14] Roshko, A. 1961 Experiments on the flow past a circular cylinder at very high Reynolds number, *Journal of Fluid Mechanics*, **10**, 345-356.

[15] Cantwell, B. & Coles, D. 1983 An experimental study of an entrainment and transport in the turbulent near wake of a circular cylinder, *Journal of Fluid Mechanics*, **136**, 321-374.

[16] Travin, A., Shur, M., Strelets, M. & Spalart, P. 1999 Detached-eddy simulations past a circular cylinder, *Flow, Turbulence and Combustion*, **63**, 293-313.

[17] Breuer, M. 2000 A challenging test case for large eddy simulation: high Reynolds number circular cylinder flow, *Internat. J. Heat Fluid Flow*, **21** 648654.

[18] Lakshimpathy, S. 2004 PANS method for turbulence: Simulations of high and low Reynolds number flows past a circular cylinder, M.S. thesis, Texas A&M University.

[19] Germano, M. 1972 Turbulence: The filtering approach, The Massachusetts Institute of Technology.

[20] Tennekes, H & Lumley, J.L. 1972 A First Course in Turbulence, *Journal of Fluid Mechanics* **238**, 325-336.

[21] Lakshmipathy, S. & Girimaji, S.S. 2007 Extension of Boussinesq turbulence constitutive relation for bridging methods, *Journal of Turbulence* **Volume 8**, N 31

[22] Reyes, D. A. 2008 PANS turbulence model: Investigation of computational and physical closure issues in flow past a circular cylinder, M.S. thesis, Texas A&M University.